We are IntechOpen,
the world's leading publisher of
Open Access books
Built by scientists, for scientists

6,900
Open access books available

186,000
International authors and editors

200M
Downloads

154
Countries delivered to

Our authors are among the

TOP 1%
most cited scientists

12.2%
Contributors from top 500 universities

BOOK CITATION INDEX
CLARIVATE ANALYTICS
INDEXED

WEB OF SCIENCE™

Selection of our books indexed in the Book Citation Index
in Web of Science™ Core Collection (BKCI)

Interested in publishing with us?
Contact book.department@intechopen.com

Numbers displayed above are based on latest data collected.
For more information visit www.intechopen.com

Chapter

Wind Energy Conversion System Modeling toward Different Approaches

Ali El Yaakoubi, Lahcen Amhaimar and Adel Asselman

Abstract

The main focus of this chapter is to modeling the different parts of the wind energy conversion system (WECS) and reviewing the different approaches used in this context. The chapter starts with the aerodynamic and the structural modeling of the *wind turbines* (WTs), and a description of the steps used to derive a linear time invariant (LTI) model. Thereafter, the chapter introduces models of the electrical actuators in the three phases (*abc*) and park phases (*dq*) reference frames, and recalls the assumptions considered. The chapter finishes by presenting the *pulse width modulation* (PWM) control strategy, the power converters and the pitch actuator models.

Keywords: wind turbines, aerodynamics modeling, structural modeling, linear time invariant model, wind turbines control

1. Introduction

Wind, which is the main driving source of the wind turbines (WTs), is characterized by speed and direction. Its origin is movements of air masses in the atmosphere due to temperature or pressure differences. In the lower layer of the atmosphere, the winds are delayed by frictional forces and obstacles that change the wind speed and direction. This is the origin of the turbulence flows. Turbulence increases with higher ground roughness and decreases with distance from the ground, which causes the wind speed to vary over a wide range of amplitudes and frequencies. The major characterization of the winds in the lower layer is that the kinetic energy is distributed in the frequency domain, which is known as the Van der Hoven spectrum [1]. According to this model, the kinetic energy is concentrated around two frequencies, which allows splitting the wind speed (v) in two components: a slowly variable deterministic component (v_m), and a rapid variable stochastic component (v_t) as expressed by Eq.(1) [2]:

$$v = v_m + v_t \qquad (1)$$

In the turbulence domain; the turbulence spectrum observed by a rotating blade element differs from that corresponding to at a fixed point, where a part of the kinetic energy moves toward higher frequencies and will concentrate around integers of rotation frequency [3]. In the stationary domain, the wind speed changes over the rotor disc due to wind shear and tower shadow effects. Wind shear is the

change in the mean wind speed with the height due to the skin friction of the earth. Tower shadow effect is the reduction of the wind speed when the wind is felt by blades when passing the tower [4].

For an expectation of the realistic WT behavior as response to its control inputs, it is required to have an accurate model of the wind field that takes into consideration all of the above mentioned characteristics. The knowledge of the mean wind speed in a site, which represents the hour to annually changes, is necessary to predict if a wind energy installation is economically profitable. The turbulence component has low impacts on the annual energy produced, while it has significant impacts on the WT dynamics and thus on the power quality produced. Generally, two wind speed profiles including the two components are often employed in literature, an effective wind speed (i.e., a single point wind speed), and a fully field wind speed (i.e., multi points wind speed over the rotor area). The effective wind speed design is based on a mathematical model, while the fully field wind speed is derived from specialized software tools such as TurbSim [5]. The effective wind speed is sufficient in the view of maximum power *capture point*, while the full field wind profile is required to simulate the effects of the aerodynamic conditions on the WT structures.

2. WECS modeling

WECS includes various multidisciplinary subsystems, which can be classified as aerodynamic, structural and electrical. The aerodynamic subsystem represents the aerodynamic model of the WT. The structural subsystems include blades, tower and drive train models. The electrical subsystems include the generator, the back-to-back converter and the system control models. In order to model the dynamic behavior of the overall system, models of the different components need to be derived and coupled consecutively.

2.1 Aerodynamic modeling

The WT aerodynamic subsystem is often modeled by using blade element momentum (BEM) theory [6]. BEM is a *quasi-steady* method, i.e., the assumed local flow conditions and the resulting aerodynamic forces depend only on the current conditions, and would change immediately with any changes in the wind field or blade movement [4]. Under the wind effects, the WT is subjected to surface forces which vary over the rotor area. By applying this theory, the aerodynamic forces acting on each element of the blades can be calculated based on the section of that element. Drag and lift forces, as mentioned above, are the main aerodynamic forces acting on the blades structures, where the lift and the drag are the perpendicular and parallel forces to the incoming flow direction respectively, as illustrated in **Figure 1**. The lift (F_L) and the drag (F_D) forces acting on each blade section based on the local *resultant air velocity* (v), and the lift (c_l) and drag (c_d) coefficients are given by Eqs. (2) and (3), respectively:

$$F_L = \frac{1}{2}c_l(\alpha, R_e)\rho bcv^2 \tag{2}$$

$$F_D = \frac{1}{2}c_d(\alpha, R_e)\rho bcv^2 \tag{3}$$

where α, R_e, b and c are local angle of attack, Reynolds number, Blade element length and chord respectively. The lift and drag coefficients are function of the local angle of attack and the Reynolds number. The angle of attack is function of the free
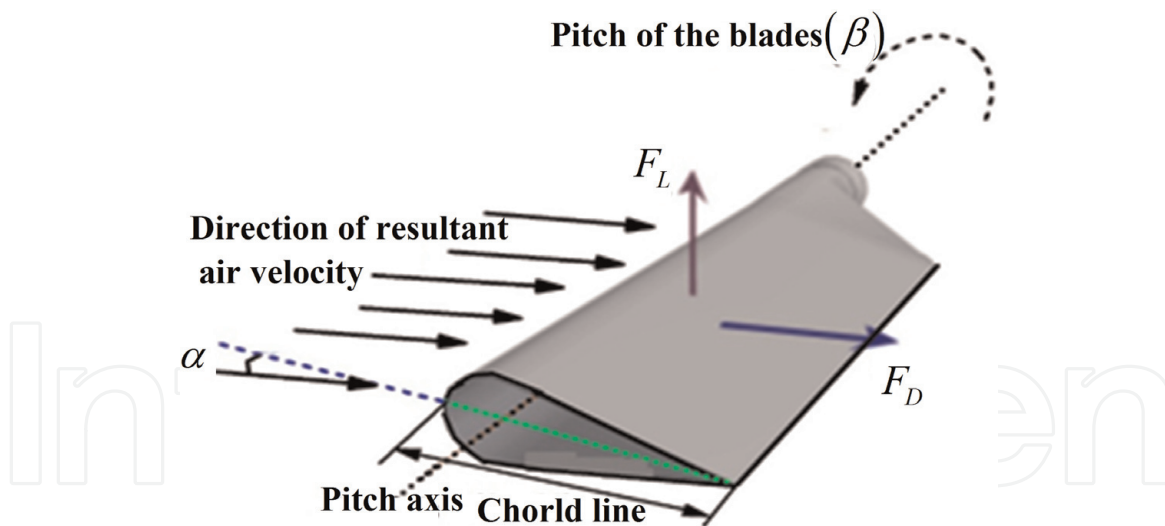
Figure 1.
Lift and drag forces on a blade.

stream wind speed, the rotational speed of the WT, and the local induction factor. The induction factor is the factor by which the free stream wind speed has been slowed down when it reaches the rotor plane. These coefficients are determined either by using wind tunnel tests or computational fluid dynamic simulations [7].

Due to the quadratic influence of the wind speed and the dependence of the lift and drag coefficients, the aerodynamic model of the WT is very complex and highly nonlinear. The lift and drag forces could be used to calculate aerodynamic torque and thrust force on the rotor, by integration from blade root to tip [7].

The aerodynamic torque and the thrust force are given by Eqs. (4) and (5), respectively.

$$T_a = \frac{1}{2}\rho\pi R^3 C_q(\lambda, \beta)v^2 \tag{4}$$

$$F = \frac{1}{2}\pi R^2 C_t(\lambda, \beta)v^2 \tag{5}$$

where C_q and C_t are torque and thrust coefficients. λ and β are tip speed ratio and pitch angle respectively. C_q and C_t can be calculated by the BEM theory, approximated by a mathematical model for simplicity and computational cost or provided by the WT manufacturer in the form of a look-up table [8]. The power coefficient is a nonlinear function of λ and β. Its value depends on the aerodynamic parameters of the turbine as well as on the metrological characteristic of the site. Theoretically this coefficient may take the value of 0.59, which is called the Betz limit, but in reality it is limited between 0.4 and 0.5 [9, 10].

For a detailed modeling, often the aerodynamic model is estimated by specialized aero-elastic simulation tools such as AeroDyn, based on the BEM theory. The outputs from the aerodynamic model are the aerodynamic thrust force and torque, and the distributed forces along each blade. These forces are considered as external forces acting on the structural components of the turbine.

2.2 Structural modeling

The structural model of the WT is a combination of flexible and rigid bodies. It includes tower, blades, drive train, nacelle, main bearing and hub. The choice of the modeling type depends strongly to the dynamics required to capture by the
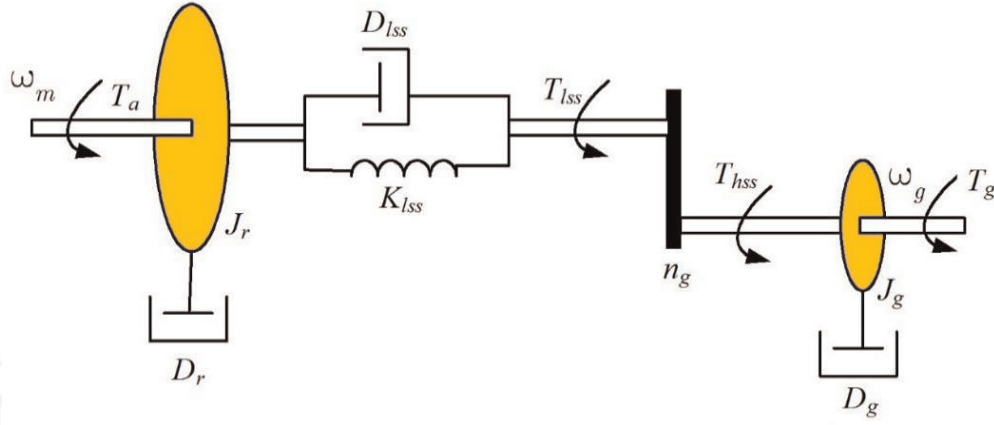
Figure 2.
Two mass model of the drive train.

model. Generally, when interesting to the WT structural dynamics often tower, blades and drive train are modeled as flexible bodies whereas the others are modeled as rigid. In contrast, when interesting to the electrical dynamics the structural dynamics can be simplified and *lumped* into one rigid mass.

2.2.1 Blades

For computational cost simplicity and modal reduction, the flexible bodies motions are assumed to be a superposition of the first eigenmodes. Usually the first and second modes are considered in simulation. This is justified by the fact, that high modes being difficult to detect in actual measurements and having negligible energy content. Therefore, each blade will be modeled by two degree of *freedoms* (DOFs) for flap-wise and one for edge-wise deflection.

2.2.2 Drive train

The drive train allows to convert the high torque with low speed (T_{lss}) to a low torque with a high speed (T_{hss}), by a set of differential equations. The dominant inertias in the WT drive train are: the rotor and generator inertias. The drive train is modeled in this *chapter* by two models: two mass and one mass. In the two mass model, the rotor and generator inertias are separated by a spring, defined by stiffness and damping coefficients, as illustrated by **Figure 2**. In the one mass model, the rotor and the generator inertias are lumped into one mass.

2.2.2.1 Two mass model

In this model, the inertias of the low speed shaft (LSS), the gearbox and the high speed shaft (HSS) are neglected compared to the inertia of the generator and the rotor. The dominant masses in this model are connected by a flexible shaft and characterized by an equivalent torsional stiffness (K_{lss}) and damping factor (D_{lss}), which would be referred either on the LSS or the HSS. The model of the drive train in this *chapter* is referred to the LSS, which is described by the following differential equations:

$$
\begin{cases}
J_r \dot{\omega}_m = T_a - T_{lss} - D_m \omega_m \\
J_g \dot{\omega}_g = T_{lss} - n_g T_{hss} - D_g \omega_g \\
T_{lss} = K_{lss}\left(\theta_m - \dfrac{\theta_g}{n_g}\right) + D_{lss}\left(\omega_m - \dfrac{\omega_g}{n_g}\right)
\end{cases}
\tag{6}
$$

where ω_m and ω_g are the rotor and the generator speed, θ_m and θ_g are the angular position of the LSS and the HSS side, J_r is the rotor inertia, J_g is the generator inertia referred to the LSS. n_g is the gearbox ratio, which is considered ideal and T_{hss} is the high shaft speed torque. D_m and D_g are the rotor and generator friction coefficient, respectively. T_g is the generator torque.

2.2.2.2 One mass model

As mentioned above, the turbine and generator inertias are lumped into one inertia in the one mass model. The one mass model referred to the LSS, is described by the following differential equation:

$$J_t \dot{\omega}_m = T_a - T_g - D_t \omega_m \qquad (7)$$

where the inertia (J_t) and the friction (D_t) coefficient of the lumped mass are expressed by:

$$\begin{cases} J_t = J_r + n_g^2 J_g \\ D_t = D_m + n_g^2 D_g \end{cases}$$

2.3 State space model of the WT

The aero-elastic equation of motion of a WT can be expressed as:

$$M(q, u, t)\ddot{q} + f(q, \dot{q}, u, u_d, t) = 0 \qquad (8)$$

where M represents the mass matrix containing inertia and mass components, and f is the nonlinear forcing function vector that includes the stiffness and damping effects. q, $\dot{q}$ and $\ddot{q}$ are the enabled DOFs displacements, velocities and accelerations. u is the control input which is the collective pitch angle, while u_d is the disturbance input. LTI (linear time invariant) model of the WT in the state space representation can be obtained by linearization of the nonlinear model by using aero-elastic software. Fatigue, aerodynamic, structural and turbulence software (FAST) linearizes numerically the equation of motion (Eq. (8)) by perturbing each variable around its respective operating point (OP) [11]. The linearization in FAST is realized in two steps. Firstly, a steady state OP of the enabled DOFs is calculated. Secondly, a numerical linearization about the resulting steady state OP is performed to form periodic matrices of the linear model. The periodic model of the WT in the state space representation, around an OP defined by the triplet $(\bar{\beta}, \bar{v}, \bar{\omega}_g)$ where $\bar{\beta}$, $\bar{\beta}$ and $\bar{\omega}_g$ the optimum value of pitch angle, wind speed and generator speed respectively, is given by:

$$\begin{cases} \dot{x}_m = A_m(\theta_m)x_m + B_m(\theta_m)u_m + B_{dm}(\theta_m)u_{dm} \\ y_m = C_m(\theta_m)x_m + D_m(\theta_m)u_m + D_{dm}(\theta_m)u_{dm} \end{cases} \qquad (9)$$

where A_m is the state matrix, B_m is the control matrix, B_{dm} is the disturbance matrix and C_m is the output matrix. The state vector is given by: $x_m = [\Delta q \ \ \Delta \dot{q}]^T$, where Δ represents the perturbation of a parameter from its optimal value. It should be noted that the matrices of the periodic state space model depend on the rotor azimuth position (θ_m). Therefore, it is important to mention that the dynamics of the model of Eq. (9) are expressed in a mixed reference coordinates, as denotes the

subscript m, i.e., rotating and fixed references coordinates. In fact, the dynamics of the blades are expressed with respect to rotating reference coordinate, while those of the nacelle and tower are expressed with respect to a fixed reference coordinate. To derive a LTI model from the periodic linear model, it is required to apply a multi-blade coordinate (MBC) transformation [12]. The transformation provides a unifying reference frame for analysis and control design, where all DOFs are expressed with respect to the same reference coordinate. Employing this transformation, the model of Eq. (9) can be transformed to a periodic model expressed in a fixed reference coordinate system:

$$\begin{cases} \dot{x}_{FR} = A_{FR}(\theta_m)x_{FR} + B_{FR}(\theta_m)u_{FR} + B_{dFR}(\theta_m)u_{dFR} \\ y_{FR} = C_{FR}(\theta_m)x_{FR} + D_{FR}(\theta_m)u_{FR} + D_{dFR}(\theta_m)u_{dFR} \end{cases} \tag{10}$$

The subscript *FR* signifies that the model is expressed in the fixed reference coordinate. The states, control inputs and outputs measurement of the model in the rotating reference coordinate are transformed to those corresponding in the fixed reference coordinate using the matrix transformation ($T_c(\theta_m)$), i.e., $x_m = T_c(\theta_m)x_{FR}$, $u_m = T_c(\theta_m)u_{FR}$ and $y_m = T_c(\theta_m)y_{FR}$. The disturbance input (u_{dm}) is not transformed because it is already expressed in the fixed reference coordinate.

$$T_c(\theta_m) = \begin{bmatrix} 1 & \cos(\theta_m) & \sin(\theta_m) \\ 1 & \cos\left(\theta_m + \dfrac{2\pi}{3}\right) & \sin\left(\theta_m + \dfrac{2\pi}{3}\right) \\ 1 & \cos\left(\theta_m + \dfrac{4\pi}{3}\right) & \sin\left(\theta_m + \dfrac{4\pi}{3}\right) \end{bmatrix} \tag{11}$$

The WT averaged periodic model over the rotor rotational period (θ_m), which is the LTI model, is expressed as:

$$\begin{cases} \dot{x} = Ax + Bu + B_d u_d \\ y = Cx + Du + D_d u_d \end{cases} \tag{12}$$

3. Actuators

The actuators aim to control WECS by receiving the desired signals from the control system and providing the real signals. They include generator, converters, pitch and yaw. The generator actuator receives a desired electromagnetic torque from the torque controller and provides a real electromagnetic torque to the drive train. The converters actuator aims to produce a current in the generator that produces a real torque that matches the desired value, by means of its control system. Generally, the electrical dynamics are much faster compared to the WT structural dynamics. Thus, they can be represented by a small communication delay between the torque demanded by the generator and the actual air-gap torque acting on the mechanical system when the structural dynamics are required. Such delay can be represented by a first order system with a small time constant. The pitch actuator receives the desired pitch angle for each blade from the pitch control, and provides the realistic pitch angle for the blade. The yaw mechanism rotates the nacelle around the vertical tower axis to place the turbine directly into the wind for a maximum power generation. Under high-speed winds, the yaw mechanism turns the blades 90° from the direction of the wind to reduce stress on internal
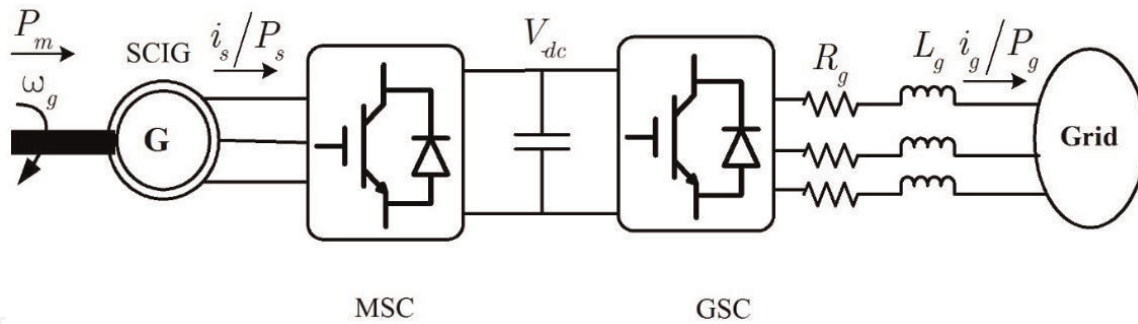
Figure 3.
SCIG interfaced to utility grid.

components and avoid over-speed conditions. The yaw actuator requires the wind inflow direction and nacelle direction as inputs, and provides the yaw angle.

As mentioned above, the pitch angle is used as control input in the full load region, while the generator torque is used as control input in the partial and the full load regions. The yaw actuator is not activated where the WT is aligned with the wind direction, to allow a maximum power capture from the wind.

3.1 Generator modeling

The generator chosen in this manuscript is squirrel *cage* induction generator (SCIG) because it is cheap, simple in construction, easy for maintenance, and easily replaceable. SCIG consists of a set of windings on the stator and rotor. The stator and rotor have three windings corresponding to the three phase system, which can be coupled either in star or delta. The stator phases of the machine are connected to the power grid through a back-to-back converter, whereas those of the rotor are short-circuited by a conductive ring at each winding side, as illustrates **Figure 3**.

3.1.1 Energy generation theory

According to Ferraris theorem, a rotating magnetic field in the gap of the machine having a sliding speed with respect to stator $(\Omega = \frac{\omega_s}{p})$ is created [13]. The rotor turns, with respect to the stator, at the mechanical speed of $\left(\omega_r = \frac{d\theta}{dt}\right)$, where θ is the angle between the stator and the rotor windings. The relative speed between the rotating field and the rotor induces a variable voltage (e_{ind}) in each closed loop of the rotor conductors, where its magnitude linked to the stator flux (Φ_s) by Faraday's law [5]:

$$\frac{d\Phi_s}{dt} = e_{ind} - R_c i_{ind} \tag{13}$$

with i_{ind} is the induced current in the conductor, and R_c is the resistance of the conductor. The stator flux linkage is defined as the flux linkage of a single turn (ϕ) multiplied by the number of turns (N) in the coils:

$$\Phi_s = N\phi$$

3.1.2 SCIG modeling assumptions

Thereafter some assumptions related to modeling of the SCIG are giving in the following of this manuscript [14]:

- The three *phase* system is symmetric and balanced with constant gap.

- The iron saturation is discarded.

- The magnetic flux density is assumed radial to the gap.

- All kind of losses in the iron are neglected.

- Both windings of the machine are sinusoidal distributed, whose axes are displaced by 120°, which produce a sinusoidal magnetic field distribution in the gap.

- The coefficients of the inductances are fixed and the coefficients of the mutual inductances depend to the windings position.

3.1.3 abc and dq0 reference frames

The quadratic-direct-zero ($dq0$) (see **Figure 4**), proposed by Park, is a reference rotating frame, for modeling and analysis of the electrical systems [15]. It allows to remove the dependency of certain parameters like inductances, and to simplify the modeling process. Generally, the electrical systems are modeled in phases reference frame. For control and analysis purposes, it is required to have the $dq0$ model of the system. The passage from a reference frame to the other is performed by means of the Park transformation matrix. By application of this transformation, the three ac (a, b and c) quantities of the generator can be reduced to two DC (d and q) components and a homopolar component.

Assuming that the dq frame is oriented by an angle (θ) from the abc reference frame, the Park transformation matrix to convert the abc quantities of the SCIG to the $dq0$ quantities is given by:

$$T(\theta) = \frac{2}{3}\begin{bmatrix} \cos(\theta) & \cos\left(\theta - \frac{2\pi}{3}\right) & \cos\left(\theta + \frac{2\pi}{3}\right) \\ \sin(\theta) & \sin\left(\theta - \frac{2\pi}{3}\right) & \sin\left(\theta + \frac{2\pi}{3}\right) \\ \frac{1}{2} & \frac{1}{2} & \frac{1}{2} \end{bmatrix} \tag{14}$$

Therefore, each quantity can be transformed from the abc to the $dq0$ reference frame by the following expression:

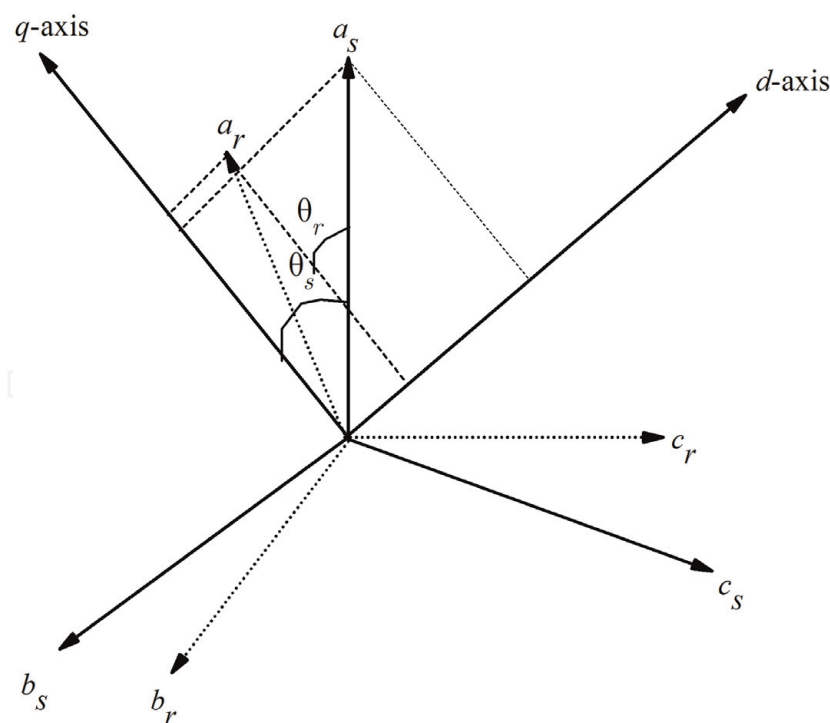$$\chi^{dq0} = T(\theta)\chi^{abc} \tag{15}$$

where χ^{dq0} and χ^{abc} are the representation of a machine parameter in the $dq0$ and abc reference frames, respectively. χ may represent voltage, current or flux of the machine.

The inverse transformation of each quantity can be recovered by means of this expression:

$$\chi^{abc} = T^{-1}(\theta)\chi^{dq0} \tag{16}$$

where

$$T^{-1}(\theta) = \begin{bmatrix} \cos(\theta) & \sin(\theta) & 1 \\ \cos\left(\theta - \frac{2\pi}{3}\right) & \sin\left(\theta - \frac{2\pi}{3}\right) & 1 \\ \cos\left(\theta + \frac{2\pi}{3}\right) & \sin\left(\theta + \frac{2\pi}{3}\right) & 1 \end{bmatrix} \tag{17}$$

Figure 4.
dqo reference frame.

3.1.4 SCIG model in the abc reference frame

Applying Faraday law's, under the above mentioned hypotheses and by using the induction motor's illustration, the dynamic model of an induction machine in the *abc* reference frame is described by the following differential equation [14, 16, 17]:

$$\left\{ \begin{matrix} v_s^{abc} \\ v_r^{abc} \end{matrix} \right\} = \begin{bmatrix} r_s^{abc} & 0 \\ 0 & r_r^{abc} \end{bmatrix} \left\{ \begin{matrix} i_s^{abc} \\ i_r^{abc} \end{matrix} \right\} + \frac{d}{dt} \left\{ \begin{matrix} \Phi_s^{abc} \\ \Phi_r^{abc} \end{matrix} \right\} \tag{18}$$

The voltage, current and flux in the *abc* reference frame are expressed as:

$$v_s^{abc} = \left\{ \begin{matrix} v_{sa} \\ v_{sb} \\ v_{sc} \end{matrix} \right\}, v_r^{abc} = \left\{ \begin{matrix} v_{ra} \\ v_{rb} \\ v_{rc} \end{matrix} \right\}, i_s^{abc} = \left\{ \begin{matrix} i_{sa} \\ i_{sb} \\ i_{sc} \end{matrix} \right\}, i_r^{abc} = \left\{ \begin{matrix} i_{ra} \\ i_{rb} \\ i_{rc} \end{matrix} \right\}, \Phi_s^{abc} = \left\{ \begin{matrix} \Phi_{sa} \\ \Phi_{sb} \\ \Phi_{sc} \end{matrix} \right\} \text{ and}$$

$$\Phi_r^{abc} = \left\{ \begin{matrix} \Phi_{ra} \\ \Phi_{rb} \\ \Phi_{rc} \end{matrix} \right\}$$

where Φ_s^{abc} and Φ_r^{abc} are the stator and rotor linkage fluxes in the *abc* reference frame, which are given by:

$$\left\{ \begin{matrix} \Phi_s^{abc} \\ \Phi_r^{abc} \end{matrix} \right\} = \begin{bmatrix} L_{ss}^{abc} & L_{sr}^{abc} \\ L_{rs}^{abc} & L_{rr}^{abc} \end{bmatrix} \left\{ \begin{matrix} i_s^{abc} \\ i_r^{abc} \end{matrix} \right\} \tag{19}$$

By which r_s^{abc}, L_{ss}^{abc}, r_r^{abc} and L_{rr}^{abc} are the resistances and inductances of the rotor and stator in the *abc* reference frame, which are expressed as:

$$
r_s^{abc} = \begin{bmatrix} r_s & 0 & 0 \\ 0 & r_s & 0 \\ 0 & 0 & r_s \end{bmatrix}, r_r^{abc} = \begin{bmatrix} r_r & 0 & 0 \\ 0 & r_r & 0 \\ 0 & 0 & r_r \end{bmatrix},
$$

$$
L_{ss}^{abc} = - \begin{bmatrix} L_s + L_m & \dfrac{-L_m}{2} & \dfrac{-L_m}{2} \\ \dfrac{-L_m}{2} & L_s + L_m & \dfrac{-L_m}{2} \\ \dfrac{-L_m}{2} & \dfrac{-L_m}{2} & L_s + L_m \end{bmatrix} \text{ and } L_{rr}^{abc} = \begin{bmatrix} L_r + L_m & \dfrac{-L_m}{2} & \dfrac{-L_m}{2} \\ \dfrac{-L_m}{2} & L_r + L_m & \dfrac{-L_m}{2} \\ \dfrac{-L_m}{2} & \dfrac{-L_m}{2} & L_r + L_m \end{bmatrix}.
$$

L_s and L_r are the inductance value of stator and rotor windings in each phase, respectively. L_m can represent the stator magnetizing inductance, the stator-rotor mutual inductance, and the rotor magnetizing inductance all referred to the stator side.

L_{sr}^{abc} and L_{rs}^{abc} are the mutual inductances between the stator and rotor phases for the rotor and stator respectively, which are expressed as:

$$
L_{sr}^{abc} = L_m \begin{bmatrix} \cos(\theta_r) & \cos\left(\theta_r + \dfrac{2\pi}{3}\right) & \cos\left(\theta_r - \dfrac{2\pi}{3}\right) \\ \cos\left(\theta_r - \dfrac{2\pi}{3}\right) & \cos(\theta_r) & \cos\left(\theta_r + \dfrac{2\pi}{3}\right) \\ \cos\left(\theta_r + \dfrac{2\pi}{3}\right) & \cos\left(\theta_r - \dfrac{2\pi}{3}\right) & \cos(\theta_r) \end{bmatrix},
$$

$$
L_{rs}^{abc} = L_m \begin{bmatrix} \cos(\theta_r) & \cos\left(\theta_r - \dfrac{2\pi}{3}\right) & \cos\left(\theta_r + \dfrac{2\pi}{3}\right) \\ \cos\left(\theta_r + \dfrac{2\pi}{3}\right) & \cos(\theta_r) & \cos\left(\theta_r - \dfrac{2\pi}{3}\right) \\ \cos\left(\theta_r - \dfrac{2\pi}{3}\right) & \cos\left(\theta_r + \dfrac{2\pi}{3}\right) & \cos(\theta_r) \end{bmatrix}.
$$

r_s and r_r are resistance value of stator and rotor windings in each phase, respectively. The induction machine coupling inductance matrix is defined by:

$$
L(\theta_r) = \begin{bmatrix} L_{ss}^{abc} & L_{sr}^{abc} \\ L_{rr}^{abc} & L_{rs}^{abc} \end{bmatrix}
$$

The rotor quantities referred to the stator are given by: $v_r^{abc} = (N_s/N_r)v_r^{abc}$, $i_r^{abc} = (N_s/N_r)i_r^{abc}$, $r_r^{abc} = (N_s/N_r)^2 r_r^{abc}$, $L_{sr}^{abc} = (N_s/N_r)^2 L_{sr}^{abc}$, $L_{rs}^{abc} = (N_s/N_r)^2 L_{rs}^{abc}$ and $L_{rr}^{abc} = (N_s/N_r)^2 L_{rr}^{abc}$. Where where N_s and N_r are the number of turns per phase in the stator and rotor windings, respectively.

The angular displacement of the rotor, with respect to the stator, and the stator are given by Eqs. (20) and (21), respectively:

$$
\theta_r(t) = \int \omega_r(t)dt + \theta_r(0) \tag{20}
$$

$$
\theta_s(t) = \int \omega_s(t)dt + \theta_s(0) \tag{21}
$$

where $\theta_r(0)$ and $\theta_s(0)$ are the initial position of the rotor and stator at t = 0, respectively. The rotor speed is linked to the mechanical speed of the generator ω_g by:

$$\omega_r = p\omega_g \tag{22}$$

The generator speed is linked to the turbine rotational speed (ω_m) by:

$$\omega_g = n_g\omega_m \tag{23}$$

3.1.5 SCIG model in dq0 reference frame

The SCIG model in the $dq0$ reference frame is obtained by applying the transformation matrices $T(\theta_s)$ and $T(\theta_s - \theta_r)$ on the abc stator and rotor parameters, respectively. Applying these transformations on the Eqs. (14) and (17) we can write

$$\begin{cases} v_s^{dq0} = T(\theta_s)r_s^{dq0}i_s^{dq0}T^{-1}(\theta_s) + T(\theta_s)\dfrac{d}{dt}\{T^{-1}(\theta_s)\Phi_s^{dq0}\} \\ v_r^{dq0} = T(\theta_s - \theta_r)r_r^{dq0}i_r^{dq0}T^{-1}(\theta_s - \theta_r) + T(\theta_s - \theta_r)\dfrac{d}{dt}\{T^{-1}(\theta_s - \theta_r)\Phi_r^{dq0}\} \end{cases} \tag{24}$$

After simplifications, the stator and rotor voltages in the $dq0$ reference frame are given by:

$$\begin{cases} v_s^{dq0} = r_s^{dq0}i_s^{dq0} + \dfrac{d}{dt}\Phi_s^{dq0} + \Omega_s\Phi_s^{dq0} \\ v_r^{dq0} = r_r^{dq0}i_r^{dq0} + \dfrac{d}{dt}\Phi_r^{dq0} + \Omega_r\Phi_r^{dq0} \end{cases} \tag{25}$$

where the voltage, the current and the flux in the $dq0$ are expressed as:

$$v_s^{dq0} = \begin{Bmatrix} v_{sd} \\ v_{sq} \\ v_{s0} \end{Bmatrix}, v_r^{dq0} = \begin{Bmatrix} v_{rd} \\ v_{rq} \\ v_{r0} \end{Bmatrix}, i_s^{dq0} = \begin{Bmatrix} i_{sd} \\ i_{sq} \\ i_{s0} \end{Bmatrix}, i_r^{dq0} = \begin{Bmatrix} i_{rd} \\ i_{rq} \\ i_{r0} \end{Bmatrix},$$

$$\Phi_s^{dq0} = \begin{Bmatrix} \Phi_{sd} \\ \Phi_{sq} \\ \Phi_{s0} \end{Bmatrix} \text{ and } \Phi_r^{dq0} = \begin{Bmatrix} \Phi_{rd} \\ \Phi_{rq} \\ \Phi_{r0} \end{Bmatrix}$$

By which Ω_s and Ω_r are the stator and rotor speed transformation matrices, which are given by: $\Omega_s = \begin{bmatrix} 0 & \omega_s & 0 \\ -\omega_s & 0 & 0 \\ 0 & 0 & 0 \end{bmatrix}$ and $\Omega_r = \begin{bmatrix} 0 & (\omega_s - \omega_r) & 0 \\ -(\omega_s - \omega_r) & 0 & 0 \\ 0 & 0 & 0 \end{bmatrix}$, respectively.

The stator and rotor resistances in the abc and $dq0$ are equal, i.e., $r_s^{dq0} = r_s^{abc}$ and $r_r^{dq0} = r_r^{abc}$.

Applying the previous transformations (Eqs. (14) and (17)), we obtain:

$$\begin{cases} T^{-1}(\theta_s)\Phi_s^{dq0} = L_{ss}^{dq0}T^{-1}(\theta_s)i_s^{dq0} + L_{sr}^{dq0}T^{-1}(\theta_s - \theta_r)i_r^{dq0} \\ T^{-1}(\theta_s - \theta_r)\Phi_r^{dq0} = L_{rs}^{dq0}T^{-1}(\theta_s - \theta_r)i_s^{dq0} + L_{rr}^{dq0}T^{-1}(\theta_s - \theta_r)i_r^{dq0} \end{cases} \tag{26}$$

After simplifications, the stator and rotor fluxes of the SCIG in the $dq0$ reference frame are given as:

$$\begin{cases} \Phi_s^{dq0} = L_{ss}^{dq0} i_s^{dq0} + L_{sr}^{dq0} i_r^{dq0} \\ \Phi_r^{dq0} = L_{rs}^{dq0} i_s^{dq0} + L_{rr}^{dq0} i_r^{dq0} \end{cases} \tag{27}$$

where $L_{ss}^{dq0} = \begin{bmatrix} L_s + \dfrac{3}{2}L_m & 0 & 0 \\ 0 & L_s + \dfrac{3}{2}L_m & 0 \\ 0 & 0 & L_{ls} \end{bmatrix}$,

$$L_{rs}^{dq0} = L_{sr}^{dq0} = \begin{bmatrix} \dfrac{3}{2}L_m & 0 & 0 \\ 0 & \dfrac{3}{2}L_m & 0 \\ 0 & 0 & \dfrac{3}{2}L_m \end{bmatrix} \text{ and } L_{rr}^{dq0} = \begin{bmatrix} L_r + \dfrac{3}{2}L_m & 0 & 0 \\ 0 & L_r + \dfrac{3}{2}L_m & 0 \\ 0 & 0 & L_r \end{bmatrix}$$

Since the rotor windings are short circuited, the abc rotor voltage components are zero, $\{v_r^{abc} = 0\}$. Moreover, as the electric system is supposed equilibrate, the electrical parameters of the model in the $dq0$ reference frame are reduced only to two components (d and q), i.e., the homopolar components equal zero ($v_{0s} = v_{0r} = i_{0s} = i_{0r} = \Phi_{0s} = \Phi_{0r}$). Therefore, the dynamic model of the SCIG machine in the dq reference frame is expressed as:

$$\begin{cases} v_{sq} = r_s i_{sq} + \dfrac{d\Phi_{sq}}{dt} + \omega_s \Phi_{sd} \\ v_{sd} = r_s i_{sd} + \dfrac{d\Phi_{sd}}{dt} - \omega_s \Phi_{sq} \\ v_{rq} = r_r i_{rq} + \dfrac{d\Phi_{rq}}{dt} + (\omega_s - \omega_r)\Phi_{rd} = 0 \\ v_{rd} = r_r i_{rd} + \dfrac{d\Phi_{rd}}{dt} - (\omega_s - \omega_r)\Phi_{rq} = 0 \end{cases} \tag{28}$$
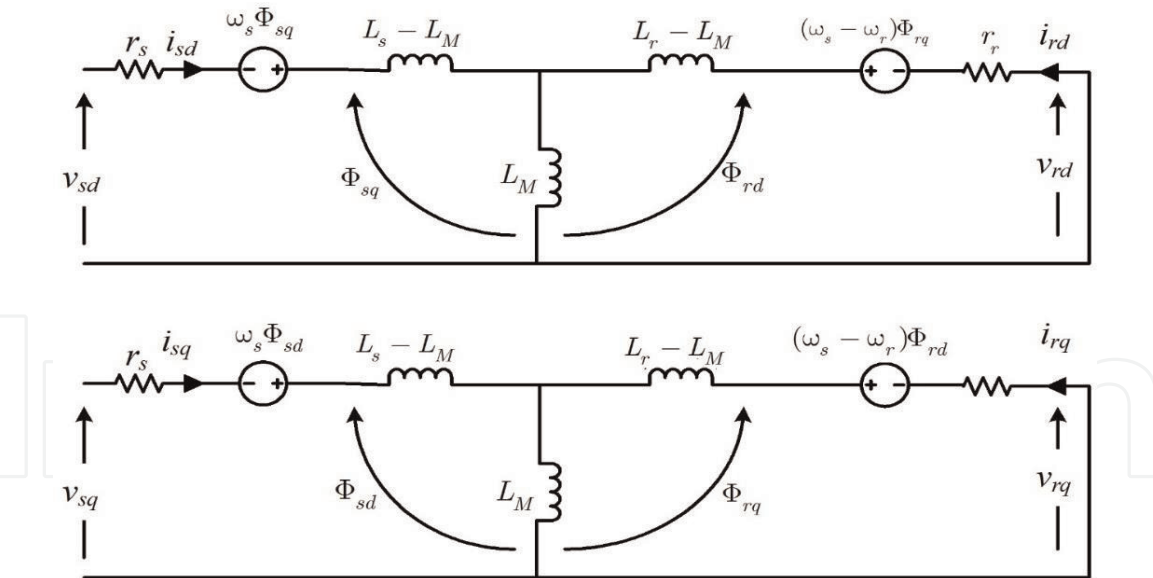
Figure 5 represents the electrical scheme of the SCIG in the dq reference frame based on the electrical model of Eq. (28).

After simplifications, the electromagnetic flux in the dq reference frame of the SCIG is given by the following equation:

$$\begin{cases} \Phi_{sq} = L_s i_{sq} + L_M i_{rq} \\ \Phi_{sd} = L_s i_{sd} + L_M i_{rd} \\ \Phi_{rq} = L_r i_{rq} + L_M i_{sq} \\ \Phi_{rd} = L_r i_{rd} + L_M i_{sd} \end{cases} \tag{29}$$

$$\text{with } \begin{cases} L_s = L_{ls} + L_M \\ L_r = L_{lr} + L_M \\ L_M = \dfrac{3}{2}L_m \end{cases}.$$

Figure 5.
Electrical scheme of the SCIG in the dq reference frame.

3.1.6 State space model of the SCIG machine in the dq0 reference frame

Combining Eqs. (28) and (29), the model of the SCIG in the state space representation can be derived, where $x_n = \left[i_{sq}, i_{sd}, i_{rq}, i_{rd}\right]^T$ is the state vector, $u_n = \left[v_{sq}, v_{sd}\right]^T$ is the control input. The state (A) and control input (B) matrices of the model are given by:

$$A = \begin{bmatrix} -\dfrac{r_s}{\sigma L_s} & \omega_s + \dfrac{p\omega_g L_m^2}{\sigma L_s L_r} & \dfrac{L_m L_r}{\sigma L_s L_r} & \dfrac{p\omega_g L_m}{\sigma L_s} \\[2ex] -\left(\omega_s + \dfrac{p\omega_g L_m^2}{\sigma L_s L_r}\right) & -\dfrac{r_s}{\sigma L_s} & -\dfrac{p\omega_g L_m}{\sigma L_s} & \dfrac{L_m L_r}{\sigma L_s L_r} \\[2ex] \dfrac{L_m r_s}{\sigma L_s L_r} & -\dfrac{p\omega_g L_m}{\sigma L_r} & -\dfrac{r_r}{\sigma L_r} & \omega_s - \dfrac{p\omega_g}{\sigma} \\[2ex] \dfrac{p\omega_g L_m}{\sigma L_r} & \dfrac{L_m L_r}{\sigma L_s L_r} & \dfrac{p\omega_g}{\sigma} - \omega_s & -\dfrac{r_r}{\sigma L_r} \end{bmatrix},$$

$$B = \begin{bmatrix} \dfrac{1}{\sigma L_s} & 0 \\[2ex] 0 & \dfrac{1}{\sigma L_s} \\[2ex] -\dfrac{L_m}{\sigma L_s L_r} & 0 \\[2ex] 0 & -\dfrac{L_m}{\sigma L_s L_r} \end{bmatrix}$$

where $\sigma = 1 - L_M^2/L_s L_r$.

3.1.7 Active power and electrical torque in the dq0 reference frame

The electromagnetic torque T_g developed by the machine depends to the instantaneous current circulated in each of the six windings and the angle between the stator and rotor windings θ. Its expression in the *abc* reference frame is given as [17]:

13

$$T_g = \frac{p}{2} \left\{ \begin{matrix} i_s^{abc} \\ i_r^{abc} \end{matrix} \right\}^T [L(\theta)] \left\{ \begin{matrix} i_s^{abc} \\ i_r^{abc} \end{matrix} \right\} \tag{30}$$

Its model in the $dq0$ reference frame is given by [14]:

$$T_g = \frac{3}{2} p \left(\Phi_{rd} i_{rq} - \Phi_{rq} i_{rd} \right) \tag{31}$$

The active power (P_s) yield by the SCIG is given as the product of the electromagnetic torque (T_g) and the generator speed (ω_g):

$$P_s = T_g \omega_g \tag{32}$$

Its expression in the $dq0$ reference frame, function of voltages and currents stator, is given by:

$$P_s = \frac{3}{2} \left(v_{sd} i_{sd} + v_{sq} i_{sq} \right) \tag{33}$$

3.2 Converters modeling

The back to back converter interfaces the WT and the utility grid. It consists of a machine side converter (MSC), which acts as rectifier, and GSC, which acts as inverter, connected by a DC link as illustrated in **Figure 6**. The DC link allows an optimum injection of the generated energy to the grid, and a frequency decoupling between the machine and the grid. The structure of the converters is bi-directional power flow, i.e., the direction of the power flow can be reversed at any time. The converter outlined in this chapter is a voltage source converter (VSC), which is a switching IGBT-diode device. Its switching model describes the steady state and the dynamic behavior, including slow transients and high frequency components of voltages and currents. The high frequency of the components are not desirable for control and analysis purposes, thus it is common to use the average value of the variables rather than the instantaneous value. Therefore, only the fundamental ac dynamics which are considered for control design and analysis [5].

The main objective associated to the rectifier is to control the WT variable speed operation, i.e., to implement the MPPT (maximum power point tracking) strategy, whereas that associated to the inverter is to manage the power flow exchanged
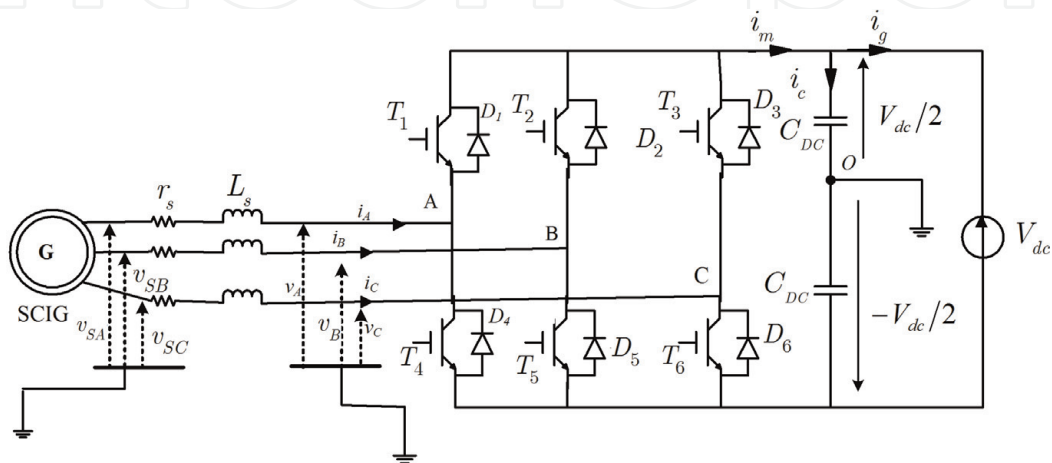
Figure 6.
MSC electrical scheme.

between the machine and the utility grid. As the modeling process of these converters are the same, we will here only to MSC. **Figure 6** illustrates the connecting scheme of the MSC to the DC link. As can be shown, each phase of the converter is composed of a set of two IGBT-diode devices connected to the DC circuit. It has been proven that the efficiency of the converter is around 94–98%, thus it is common practice to represent the back to back converters as ideal switches. Therefore, each set of the IGBT-diode of the phase will be represented by a single switch, where its switches states are complementary. Moreover, for analysis purpose, it is assumed that there is a common point in the DC link that splits the voltage V_{dc} into two voltages of amplitudes $V_{dc}/2$ [17].

3.2.1 MSC modeling assumptions

Thereafter are recalled some assumptions related to the converter modeling [14]:

- The switching of the components is instantaneous.

- The voltage drops at their terminals are negligible.

- The dead times are neglected.

- The load is three-phase balanced and coupled in star with isolated neutral point.

- It is assumed that the IGBTs switch at a frequency at least 10 times of the fundamental frequency of the ac grid, thus the action of this commutation can be represented by the average of the duty cycle [5]. Therefore, the currents and voltages of the VSC are expressed as function of the duty cycle of the IGBT.

3.2.2 MSC model in abc *reference frame*

Applying Kirchhoff's law to circuit given in **Figure 6**, the compound voltages between the three phases at the right side, are:

$$\begin{cases} u_{AB} = u_{AO} - u_{BO} \\ u_{BC} = u_{BO} - u_{CO} \\ u_{CA} = u_{CO} - u_{AO} \end{cases} \tag{34}$$

At the load side, the compound voltages are function of the simple voltages, i.e., the voltages between the phases A, B and C and the point O, are expressed as:

$$\begin{cases} u_{AB} = v_A - v_B \\ u_{BC} = v_B - v_C \\ u_{CA} = v_C - v_A \end{cases} \tag{35}$$

The voltages equations of the VSC can be expressed also as [17]:

$$\begin{cases} u_{AB} - u_{CA} = 2v_A - (v_B + v_C) \\ u_{BC} - u_{AB} = 2v_B - (v_C + v_A) \\ u_{CA} - u_{BC} = 2v_C - (v_A + v_B) \end{cases} \tag{36}$$

Moreover, as the voltages v_A, v_B, v_C form an equilibrium three phase system, the expression of Eq. (36) can be reduced to [5]:

$$\begin{cases} u_{AB} - u_{CA} = 3v_A \\ u_{BC} - u_{AB} = 3v_B \\ u_{CA} - u_{BC} = 3v_C \end{cases} \qquad (37)$$

Thus, the simple voltages function of the voltages between the phases and the effective point O, are expressed by:

$$\begin{cases} v_A = \dfrac{1}{3}(u_{AB} - u_{CA}) \\ \\ v_B = \dfrac{1}{3}(u_{BC} - u_{AB}) \\ \\ v_C = \dfrac{1}{3}(u_{CA} - u_{BC}) \end{cases} \qquad (38)$$

$$\begin{bmatrix} v_A \\ v_B \\ v_C \end{bmatrix} = \frac{1}{3} \begin{bmatrix} 2 & -1 & -1 \\ -1 & 2 & -1 \\ -1 & -1 & 2 \end{bmatrix} \begin{bmatrix} u_{AO} \\ u_{BO} \\ u_{CO} \end{bmatrix} \qquad (39)$$

As mentioned above, each phase is formed by two complementary ideal switches, i.e., if we associate to each phase a binary value of command S_i (i = A, B, C) we have:

S_i = +1, the upper switch is on and the lower switch is off;
S_i = −1, the upper switch is off and the lower switch is on.

Therefore, the voltages between the phases and the effective point O, function of the switch functions and the DC link voltage are derived

$$\begin{bmatrix} u_{AO} \\ u_{BO} \\ u_{CO} \end{bmatrix} = \frac{V_{dc}}{2} \begin{bmatrix} S_A \\ S_B \\ S_C \end{bmatrix} \qquad (40)$$

Combining Eqs. (39) and (40), the simple phase voltages, function of the switching functions and the DC link voltage, are obtained:

$$\begin{bmatrix} v_A \\ v_B \\ v_C \end{bmatrix} = \frac{1}{3} \begin{bmatrix} 2 & -1 & -1 \\ -1 & 2 & -1 \\ -1 & -1 & 2 \end{bmatrix} \frac{V_{dc}}{2} \begin{bmatrix} S_A \\ S_B \\ S_C \end{bmatrix} \qquad (41)$$

Finally, the simple voltages of the three phases at the output of the converter are given function of the switch functions. The switching functions are the commands of the converter, where their states will be provided from PWM control strategy.

Moreover, applying Kirchhoff's law at the load side, the average model of the VSC, in the *abc* reference frame is given by:

$$\begin{cases} L_s \dfrac{di_A}{dt} + r_s i_A = v_{SA} - v_A \\ \\ L_s \dfrac{di_B}{dt} + r_s i_B = v_{SB} - v_B \\ \\ L_s \dfrac{di_C}{dt} + r_s i_C = v_{SC} - v_C \end{cases} \qquad (42)$$

where v_{SA}, v_{SB} and v_{SC} are the induced voltages in the stator phases of the generator.

3.2.3 MSC model in the dq0 reference frame

Expressing the voltages and currents of the VSC in the *dq* reference frame allows controlling independently the electromagnetic torque and rotor flux.

The model of the MSC in the *dq0* reference frame can be obtained by application of the transformation matrix of Eq. (14) on Eq. (42) [8]:

$$
\begin{cases}
L_s \dfrac{di_{sd}}{dt} + r_s i_{sd} = v_{sd} - S_d \dfrac{V_{dc}}{2} \\[2mm]
L_s \dfrac{di_{sq}}{dt} + r_s i_{sq} = v_{sq} - S_q \dfrac{V_{dc}}{2}
\end{cases}
\tag{43}
$$

where S_d and S_q are the *d* and *q* switch functions, respectively.

This model will be used to control the SCIG machine by controlling the VSC based on PWM control strategy. Selective harmonic elimination, sinusoidal pulse width modulation (SPWM) and space vector modulation are the commonly found PWM strategies in literature. SPWM is the most used due to its simplicity and effectiveness [5].

3.2.4 SPWM control strategy

SPWM is a multi-pulses-based modulation method that varies the pulse width of the converter output voltage in a sinusoidal manner, following a target reference voltage by comparing a low frequency reference signal (f_m) with a high frequency carrier signal (f_p), where $f_m \ll f_p$ [5]. The frequency of the reference signal should equal the frequency of the output voltage. For each phase leg, there are two complementary standing signals, one for the lower switch and the other for the upper switch. In fact, when the reference signal exceeds the carrier signal, the upper switch is turned on and the lower switch is off. Otherwise if the reference signal is less that the carrier signal, the lower switch is turned on and the upper switch is turned off.

For a three phase VSC, the three phase reference signals v_{mA}, v_{mB}, and v_{mC} and a high frequency carrier (v_p) are used
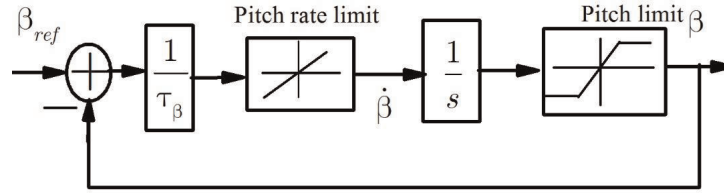
$$
\begin{cases}
v_{mA} = \hat{V}_m \sin\left(2\pi f_m t\right) \\[2mm]
v_{mB} = \hat{V}_m \sin\left(2\pi f_m t - \dfrac{2\pi}{3}\right) \\[2mm]
v_{mC} = \hat{V}_m \sin\left(2\pi f_m t + \dfrac{2\pi}{3}\right)
\end{cases}
\tag{44}
$$

$$
v_p =
\begin{cases}
\hat{V}_p \left(-1 + 4\dfrac{t}{T_p}\right) \\[2mm]
\hat{V}_p \left(3 - 4\dfrac{t}{T_p}\right)
\end{cases}
\text{if}
\begin{cases}
t \in \left[0, \dfrac{T_p}{2}\right] \\[2mm]
t \in \left[\dfrac{T_p}{2}, 0\right]
\end{cases}
$$

where $\hat{V}_m$ and $\hat{V}_p$ are the voltages amplitude, and T_p is the period of the carrier. The states of the IGBT (S_j) (j = 1,2,3) are derived as follow:

$$
S_j =
\begin{cases}
+1 \\
-1
\end{cases}
\text{if}
\begin{cases}
v_{mi} - v_p \geq 0 \\
v_{mi} - v_p < 0
\end{cases}
$$

Figure 7.
Pitch actuator scheme.

where the states of the lower switches will be complementary with those of the upper switches. Thus the simple voltages (v_i) at the terminal of the converter are:

$$v_i = \begin{cases} +\dfrac{V_{dc}}{2} \\ -\dfrac{V_{dc}}{2} \end{cases} \text{if} \begin{cases} S_j = +1 \\ S_j = -1 \end{cases}$$

Therefore, the voltages at the output of the converter are a set of rectangular slots, whose width varies as function of the control law of the IGBT, the duration of switch and the time of functioning. Two parameters characterize this control strategy: the modulation index, which is the ratio of f_m and f_p; and the tuning coefficient, which is the ratio of $\hat{V}_m$ and $\hat{V}_p$. For a proper control, these coefficients must be tuned carefully. Various works are interested to WTs control either for maximum capture, power flow exchange as well as power regulation and structural loads minimization. Readers can refer to [18–23].

3.3 Pitch actuator

The pitch actuator system aims to drive the blades to the desired positions received from the pitch control. Due to the large inertia of the blades, there is a significant delay between a blade pitch command and the blade actually arriving in the desired position. The actuator dynamics are largely dominated by the blades and the motor inertias, and the capabilities of the pitch system; while the torque caused by the aerodynamic loading of the blades has only small impacts. Often the pitch actuator model is linear first order system with low pass filter, additional rate limiter acting on the demanded pitch angle $\left(\beta_{ref}\right)$ and angle limiter to set the maximum and the minimum pitch angles. The pitch system can be either hydraulic, electromechanical, or a hybrid of the both. Eq. (45) represents the model of the actuator, where τ_β is the time constant of the model.

$$\frac{\beta}{\beta_{ref}} = \frac{1}{\tau_\beta.s + 1} \tag{45}$$

Figure 7 illustrates the pitch actuator scheme based on the mathematical model of Eq. (45).

4. Conclusions

This chapter presented the different models of the WECS such as wind turbines aerodynamics and structural dynamics, generator and converter actuators. The chapter has outlined the hypotheses and the approaches used in control and

modeling such as state space representation, and the *abc* and the *dq* reference frames. The chapter finished by presentation of the SPWM control strategy and the pitch angle actuator.

Conflict of interest

The authors do not have any conflicts of interest to declare.

Nomenclature

abc	three phases system
dq	park phases
θ_s	position angle between the *abc* and the *dq* reference frames
θ_r	position angle between the rotor and the stator windings in the *abc* reference frame
a_r, b_r, c_r	rotor windings axes in the *abc* reference frame
a_s, b_s, c_s	stator windings axes in the *abc* reference frame
P_s	electrical power
T_g	electromagnetic torque
ω_g	generator speed
i_s	stator current
P_g	electrical energy injected to grid
L_g	filter inductance
R_s	filter resistances
i_g	grid current
V_{dc}	DC link voltage
MSC	machine side converter
GSC	grid side converter
VSC	voltage source converter

Author details

Ali El Yaakoubi*, Lahcen Amhaimar and Adel Asselman
Optic and Photonic Team, Abdelmalek Essaadi University, Tetouan, Morocco

*Address all correspondence to: ali.elyaakoubi@gmail.com

IntechOpen

References

[1] Van der Hoven I. Power spectrum of horizontal wind speed in the frequency range from 0.0007 to 900 cycles per hour. Journal of Meteorology. 1957;**14**: 160-164. DOI: 10.1175/1520-0469(1957) 014<0160:PSOHWS>2.0.CO;2

[2] Nichita C, Luca D, Dakyo B, Ceanga E. Large band simulation of the wind speed for real time wind turbine simulators. IEEE Transactions on Energy Conversion. 2002;**17**:523-529. DOI: 10.1109/TEC.2002.805216

[3] Bianchi FD, de Battista H, Mantz RJ. Wind Turbine Control Systems: Principles, Modelling and Gain Scheduling Design. London: Springer-Verlag; 2007

[4] Arne K. Extreme and fatigue load reducing control for wind turbines: A model predictive control approach using robust state constraints [thesis]. Berlin: von der Fakultät III—Prozesswissens der Technischen Universität Berlin; 2014

[5] El Yaakoubi A. Wind energy conversion systems control for maximum power capture and excessive loads alleviation [thesis]. Tétouan, Morocco: Abdelmalek Essaadi University; 2018

[6] Hansen MOL. Aerodynamics of Wind Turbines. 3rd ed. New York, NY: Routledge; 2015

[7] Ingram G. Wind turbine blade analysis using the blade element momentum method. version 1.0 [thesis]. UK: School of Engineering, Durham University; 2005

[8] Munteanu I, Bratcu AI, Cutululis N-A, Ceanga E. Optimal Control of Wind Energy Systems: Towards a Global Approach. London: Springer-Verlag; 2008

[9] Chen Z, Guerrero JM, Blaabjerg F. A review of the state of the art of power electronics for wind turbines. IEEE Transactions on Power Electronics. 2009;**24**:1859-1875. DOI: 10.1109/TPEL.2009.2017082

[10] Ragheb M, Ragheb AM. Wind turbines theory—The betz equation and optimal rotor tip speed ratio. In: Carriveau R, editor. Fundamental and Advanced Topics in Wind Power. IntechOpen; 2011. DOI: 10.5772/21398

[11] Jonkman JM, Buhl ML Jr. Fast user's guide-updated August 2005 [Technical Report]. Golden-Colorado: National Renewable Energy Laboratory (NREL); 2005

[12] Bir GS. User's guide to mbc3: Multi-blade coordinate transformation code for 3-bladed wind turbine [Technical Report]. Golden-Colorado: National Renewable Energy Laboratory (NREL); 2010

[13] El Aimani S. Modélisation des différentes technologies d'éoliennes intégrées dans un réseau de moyenne tension [thesis]. Ecole Centrale de Lille; 2004

[14] García D. Modeling and control of squirrel cage induction generator with full power converter applied to windmills [thesis]. Spain: Escola Tècnica Superior d'Enginyeria Industrial de Barcelona—Enginyeria Industrial; 2009

[15] Park RH. Two-reaction theory of synchronous machines generalized method of analysis—Part I. Transactions of the American Institute of Electrical Engineers. 1929;**48**:716-727. DOI: 10.1109/T-AIEE.1929.5055275

[16] Fateh F. Nonlinear control schemes for extremum power seeking and

torsional vibration mitigation in variable speed wind turbine systems [thesis]. USA: Kansas State University; 2015

[17] Olimpo A-L, David C-G, Edgar M-G, Grain A. Offshore Wind Energy Generation: Control, Protection, and Integration to Electrical Systems. Chichester: John Wiley & Sons Ltd; 2017

[18] Yaakoubi AE, Hajri MEH, Attari K, Amhaimar L, Asselman A. Advanced control strategies of SCIG based wind turbines for MPPT. In: Proceedings 3rd International Conference Smart City Applications; New York, NY, USA: ACM; 2018. pp. 36:1-36:5. DOI: 10.1145/3286606.3286813

[19] Yaakoubi AE, Amhaimar L, Attari K, Harrak MH, Halaoui ME, Asselman A. Non-linear and intelligent maximum power point tracking strategies for small size wind turbines: Performance analysis and comparison. Energy Reports. 2019;**5**:545-554. DOI: 10.1016/j.egyr.2019.03.001

[20] El Yaakoubi A, Attari K, Asselman A, Djebli A. Novel power capture optimization based sensorless maximum power point tracking strategy and internal model controller for wind turbines systems driven SCIG. Frontiers in Energy. 2017. DOI: 10.1007/s11708-017-0462-x (Article in press)

[21] Yaakoubi AE, Attari K, Amhaimar L, Asselman A. Adaptive state feedback pitch angle control of wind turbines for speed regulation and blades loadings alleviation. International Review of Automatic Control IREACO. 2018;**11**:174-187. DOI: 10.15866/ireaco.v11i4.14503

[22] El Yaakoubi A, Attari K, Asselman A, Djebli A. Simulation and investigation of the behavior of a large-scale direct driven wind turbine connected to the grid. UPB Scientific Bulletin, Series C: Electrical

Engineering. 2017;**79**:241-252. DOI: 10.1016/j.egyr.2016.10.004

[23] Yaakoubi AE, Asselman A, Djebli A, Aroudam EH. A MPPT strategy based on fuzzy control for a wind energy conversion system. Procedia Technology. 2016;**22**:697-704. DOI: 10.1016/j.protcy.2016.01.145